Physical chemical properties of geomaterials

Bublikova T.M., Setkova T.V., Drozhzhina N.A., Nekrasov A.N., Balitsky V.S. Experimental study of the mechanism of malachite leaching by ammonium hydroxide solutions. *UDC 549.743.12:546.171.1*

D.S. Korzhinskii Institute of Experimental Mineralogy RAS, Chernogolovka *tmb@iem.ac.ru*

Abstract. Experimental study of the reaction of interaction of basic copper carbonates with ammonia solutions was carried out in recirculation-evaporation reactors of IEM RAS design. Powder malachite (particle size 5–10 μm) and crushed synthetic malachite with particle size 5–7 mm were selected as objects of study. Ammonia solutions with a concentration of 2.0 m NH_3 were used in the experiments. The dissolution temperature of basic copper carbonates was maintained at 40–50 °C. It is shown that tenorite formation is a limiting stage in the process of leaching of basic copper carbonates. By the method of X-ray phase analysis it was established that during the interaction of ammonia solutions with bulk particles of crushed malachite intermediate phases crystallize on the surface of malachite grains*: carbonate diammine copper* $[Cu(NH_3)_2CO_3]$ and carbonate tetraammine copper $[Cu(NH_3)_4CO_3]$.

Keywords: *basic copper carbonate, malachite, ammonia solutions, recirculation crystallizer, diammine copper carbonate, tetraammine copper carbonate*

Introduction. Hydrometallurgical methods of processing depleted ores and secondary waste are becoming increasingly important in the extraction of non-ferrous metals. Such methods are preferred for copper extraction because pyrometallurgical methods are more complex and less environmentally friendly. Diluted solutions of sulfuric acid are often used as a leaching agent in hydrometallurgy. However, if the rock contains a large amount of carbonates or hydroxides [$CaCO_3$, $MgCO_3$, $Al(OH)_3$, $Ca(OH)_2$], the acid consumption increases sharply, the process becomes ineffective, and metallurgical treatment is economically unprofitable (Ekmekyapar et al., 2012; Radmehr et al., 2014; Lin et. al., 2023). Recent studies have shown that ammonium hydroxide solutions may be promising for copper extraction at high content of oxide and basic copper carbonate in the rock (Wang et al., 2009; Aracena et al., 2015, 2020; Panayotova et al., 2017; Nadirov et al., 2017). The relevance of research into the interaction of copper minerals with ammonia solutions is determined by the need to select optimal parameters and improve hydrometallurgical processes for copper extraction.

The efficiency of using ammonia in leaching processes depends on many factors: the composition of copper ores, the composition and pH of solutions, leaching time, the solid-to-liquid ratio, leaching temperature, the size of rock particles, etc. (Oudenne et. al., 1983; Arzutug et al., 2004; Aracena et al., 2020; Velásquez-Yévenes et al., 2022). Some details of the chemistry of complex aqueous copper-ammonia systems are not well understood or require clarification to obtain maximum copper recovery.

The aim of this work is an experimental study of the reaction of interaction of basic copper carbonates with aqueous ammonia solutions. Malachite $[Cu_2CO_3(OH)_2]$ was chosen as the object in the model system. It is a basic copper carbonate and is one of the 15 important copper-containing minerals of industrial significance.

Experiment and research methods. The experiments were carried out in recirculation-evaporation reactors designed by the IEM RAS (Bublikova et al., 2000). The steel reactor (volume 800 ml) is equipped with a heating element, a water cooling system and a basket for the charge. As a result of heating, a constant circulation of the solution occurs in the reactor. The solution accumulates in the charge basket and interacts with the charge material. The charge material consisted of basic copper carbonate ($Cu_2CO_3(OH)_2$) with a particle size of 5–10 μm or crushed synthetic malachite with a piece size of 5–7 mm. Synthetic malachite was obtained using the method developed at the IEM RAS (Bublikova et al., 2019). The charge material was characterized using X-ray phase analysis (Fig. 1).

The phase composition of the obtained samples was studied by X-ray phase analysis on a Bruker «D2 Phaser» diffractometer. The morphology, internal structure and elemental composition of the samples were analyzed using a Tescan Vega II XMU scanning *microscope* with an INCA Energy 450 energy-dispersive spectrometer (EDS). The samples were sputtered with gold (layer thickness 3 nm).

Results of the experiments and discussion. The results of a study of the kinetics of malachite leaching with ammonia solutions, conducted by P. Oudenne and A. Olson (Oudenne, Olson, 1983), showed that the dissolution process includes two stages. The first stage is the actual chemical dissolution with the transition of copper into the solution. But after ~ 10% of the reaction the rate decreased due to the formation of an intermediate phase in the porous layer of malachite grains, presumably copper hydroxide $Cu(OH)_2$. This phase subsequently dissolves in excess ammonia, but makes it difficult to dissolve malachite.

For experimental modeling of the malachite leaching process, we conducted two series of

experiments on the interaction of basic copper carbonates with ammonia solutions. The main parameters of the experiments were the same in both series: heating temperature 70–80 °C; charge dissolution temperature 40–50 °C; saturated ammonia vapor pressure, ammonia concentration 2.0 m NH_3; experiment duration 12 days. The fundamental difference between the series of experiments was in the particle sizes of the charge material. The particles of the basic copper carbonate reagent were 5–10 μm in size, while the pieces of crushed malachite were 5–7 mm.

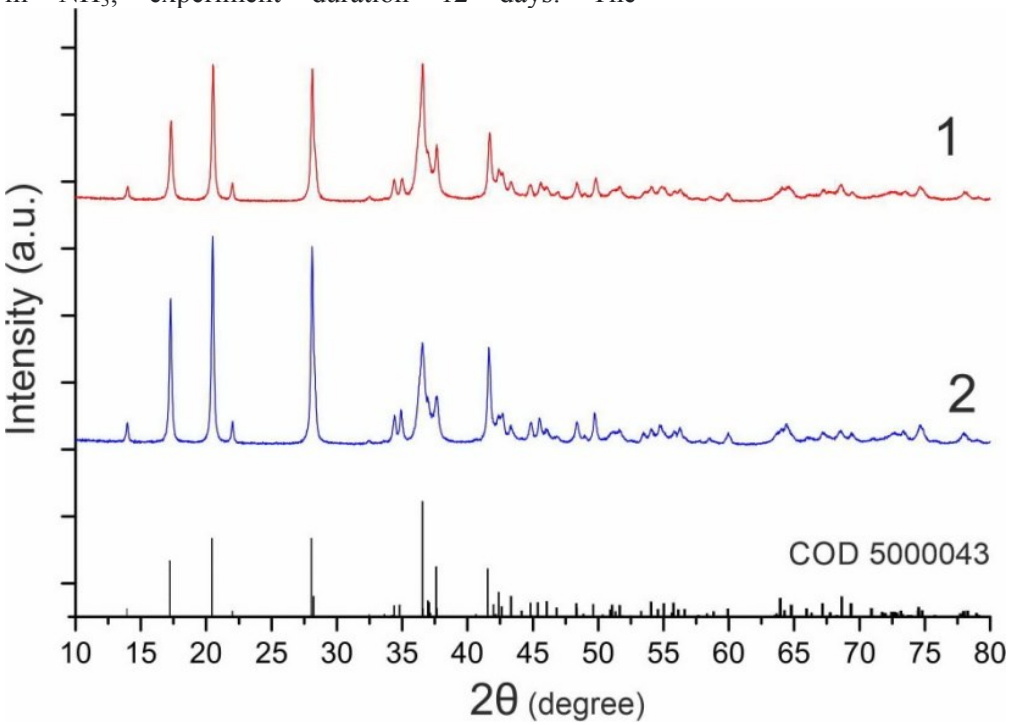

Fig. 1. XRD powder diffraction pattern of the charge material: 1 – chemical reagent basic copper carbonate [$Cu_2CO_3(OH)_2$]; 2 – synthetic malachite**.**

In the first series of experiments, the condensing solution dripped onto the surface of the charge; a dense layer of the charge retained part of the solution, and it accumulated in the basket. The basic copper carbonate reagent was dissolved in an ammonia solution. The malachite dissolved incongruently with the formation of the tenorite phase (Fig. 2a, 3a). Previously, we established that the solubility of malachite in 2.0 m NH_3 at temperatures 40 - 50 °C is one and a half orders of magnitude greater than that of tenorite. (Bublikova et al., 2025). New portions of the solution continued to enter the charge, but the process of charge dissolution slowed down. The formation of the tenorite phase limited the process of leaching of the charge basic copper carbonate. After the experiments are completed, a mixture of tenorite and malachite crystalline phases is present in the charge basket. The diffraction pattern of the studied samples demonstrates that other phases in the charge material are absent (Fig. 3a).

In the second series of experiments, the reaction mechanism of the charge dissolution changed. The ammonia solution entering the basket dripped onto the crushed malachite and dissolved primarily the surface layer of the bulk pieces of malachite. As a result of the incongruent dissolution of malachite, tenorite was also formed. The reaction products contain other visually distinguishable phases (Fig. 2b), most of which are represented by blue-violet crystals of prismatic appearance. The crystal faces are cracked, the edges are smoothed. As a result of the action of new portions of the ammonia solution, the crystals partially dissolved and lost their original appearance (Fig. 2c).

Thermodynamic calculations of the phase formation conditions in aqueous copper-carbonate systems have shown that when malachite is dissolved in ammonium hydroxide 2.0 m NH_3 at temperatures of 20–100 °C, the dissolved copper is in the form of copper-ammonia complexes $Cu(NH_3)_n^{2+}$ (n=2–5), predominantly $Cu(NH_3)_4^{2+}$. The quantitative ratios of the complexes depending on the temperature (Bublikova et al., 2025). In general, the reaction of malachite interaction with ammonia solutions can be expressed by the equation:

$$Cu_2CO_3(OH)_2(s) + 2nNH_3(aq) \rightarrow$$
$$2Cu(NH_3)_n^{2+}(aq) + CO_3^{2-}(aq) + 2OH^-(aq)$$

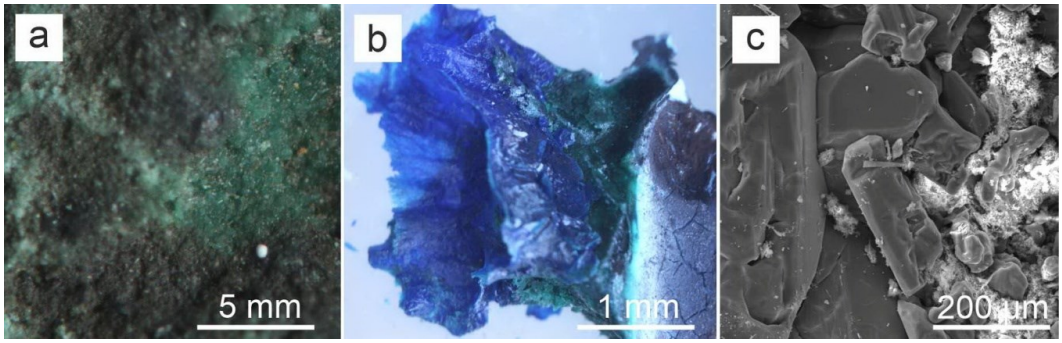

Fig. 2. Photo under a microscope: a – mixture of tenorite and malachite phases, b – *carbonate diammine copper* [$Cu(NH_3)_2\,CO_3$] and *carbonate tetraammine copper* [$Cu(NH_3)_4\,CO_3$]; c – SEM image of crystals [$Cu(NH_3)_2\,CO_3$] and [$Cu(NH_3)_4\,CO_3$].

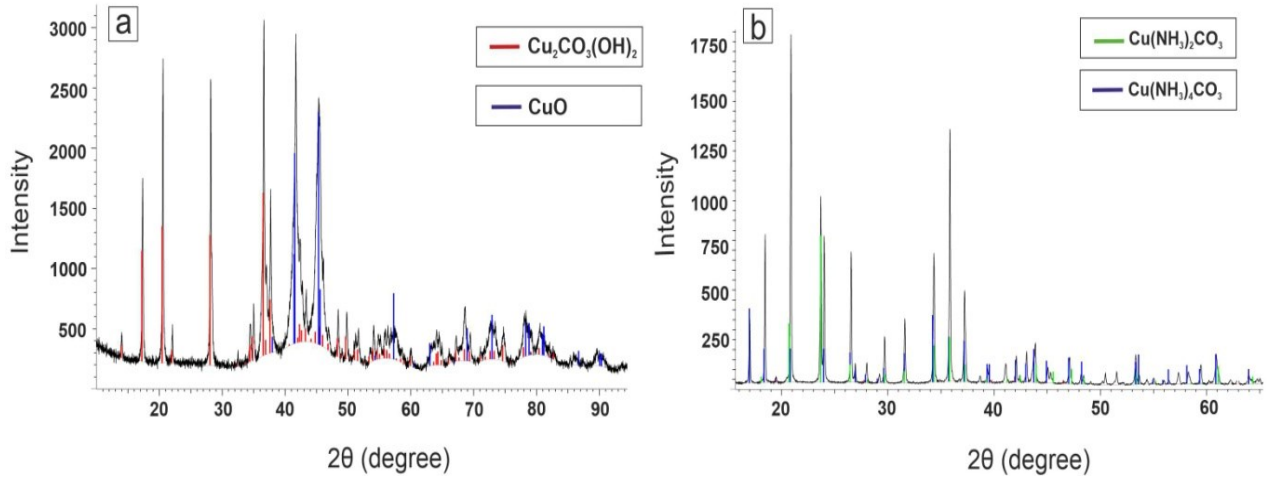

Fig. 3. XRD powder diffraction pattern of a – tenorite (CuO) and basic copper carbonate malachite [$Cu_2CO_3(OH)_2$]; b – *carbonate diammine copper* [$Cu(NH_3)_2\,CO_3$] *and carbonate tetraammine copper* [$Cu(NH_3)_4\,CO_3$].

Obviously, that the presence of carbonate ion in the solution creates possible conditions for the formation of complex salts of copper and ammonia. To determine the composition of the crystalline phase formed on the surface of malachite, we selected blue-violet crystals and carefully cleaned them from traces of tenorite and malachite. After the experiments were completed, X-ray phase analysis revealed the presence of a mixture of crystalline phases in the composition of the charge. The intensity and position of the diffraction peaks on the diffraction pattern indicate that two phases are present in the selected samples of the charge: carbonate diammine copper [$Cu(NH_3)_2CO_3$] (PDF card No. 00–026–0507) (Meyer et al., 1972) and carbonate tetraammine copper [$Cu(NH_3)_4CO_3$] (PDF card No. 00–003–0217) (Fig. 3b). Copper hydroxide $Cu(OH)_2$ was not detected in the studied samples.

Conclusion. The conducted experimental study of the reaction of interaction of basic copper carbonates with ammonia solutions made it possible to identify some features of the malachite leaching process. It was established that under the experimental conditions (ammonia concentration 2.0 m NH_3, charge dissolution temperature 40–50 °C), the dissolution of the basic copper carbonate $Cu_2CO_3(OH)_2$ with particle sizes of 5–10 μm occurs in one stage, with the formation of tenorite. With an increase in the particle size of the charge malachite to 5–7 mm, the dissolution reaction mechanism becomes more complex. Along with tenorite, crystallization of intermediate phases of carbonate diammine copper [$Cu(NH_3)_2CO_3$] and carbonate tetraammine copper [$Cu(NH_3)_4CO_3$] occurs on the surface of crushed malachite grains. These phases block the surface layer of the charge material and slow down the malachite leaching process. Grinding malachite ore to the micron level increases the speed of the ammonia leaching process due to the larger surface area of the malachite particles and the absence of intermediate phases, such as complex salts of copper and ammonia.

This study is fulfilled under Research program № FMUF-2022-0002 of the Korzhinskii Institute of Experimental Mineralogy.

References

Aracena A., Vivar Y., Jerez O., Vásquez D. Kinetics of dissolution of tenorite in ammonium media // Mineral Processing and Extractive Metallurgy Rev. 2015. V. 36. P. 317. https://doi.org/10.1080/08827508.2015.1004404.

Aracena A., Pino J., Jerez O. Mechanism and kinetics of malachite dissolution in an NH_4OH system // Metals. 2020. № 10. P. 833. https://doi.org/10.3390/met10060833.

Arzutug M. E., Kocakerim M. M. Leaching of malachite ore in NH_3-saturated water // Ind. Eng. Chem. Res. 2004. № 43. P. 4118–1423. https://doi.org/10.1021/ie0342558.

Bublikova T.M., Balitsky V.S., Timokhina I.V. Synthesis and main properties of jewelry and ornametal malachite. Synthesis of minerals. V. 1. Alexandrov, VNIISIMS. 2000. 662 p. (In Russian).

Bublikova T.M., Balitsky V.S., Khanin D.A., Nekrasov A.N., Setkova T.V. Features of the internal structure of a synthetic malachite // Moscow university geology bulletin. 2019. V. 74. № 1. P. 73-80. https://doi.org/10.3103/S0145875219010034.

Bublikova T.M., SetkovaT.V., Balitsky V.S. Thermodynamic Modeling of Phase Formation Conditions in the $CuO–CO_2–H_2O–NH_3$ System // Russian Journal of Inorganic Chemistry. 2025. Vol. 70. № 1. P. 78–87. https://doi.org/10.1134/S0036023624602599.

Ekmekyapar A., Aktaş E., Cüncül A., Demirkiran N. Investigation of leaching kinetics of copper from malachite ore in ammonium nitrate solutions // Metallurgical and materials transactions B. 2012. V. 43B. P. 764–772. https://doi.org/10.1007/s11663-012-9670-2.

Lin P., Werner J., Ali Z.A., Bertucci L., Groppo J. Kinetics and Modeling of Counter-Current Leaching of Waste Random-Access Memory Chips in a Cu-NH_3-SO_4 System Utilizing Cu(II) as an Oxidizer // Materials 2023. V. 16. P. 6274. https://doi.org/10.3390/ ma16186274.

Meyer M.H., Singh P., Hatfield W.E., Hodgson D.J. The crystal and molecular structure of carbonatodiamminecopper (II), $Cu(NH_3)_2CO_3$ // Acta Cryst. 1972. B28. P. 1607−1613.

Nadirov R., Syzdykova L, Zhussupova A. Copper smelter slag treatment by ammonia solution: Leaching process optimization // J. Cent. South Univ. 2017. V. 24. P. 2799−2804.

Oudenne P.D., Olson A.F. Leaching kinetics of malachite in ammonium carbonate solutions // Metallurgical Transactions .1983. V. 14B. P. 33−40. https://doi.org/10.1007/BF02670866.

Panayotova M., Panayotov V. Copper recovery from low grade ores, concentrates and technogenic waste by ammonia leaching - an old idea with promising future // Journal scientific and applied research. 2017. Vol. 11. P. 10.

Radmehr V., Koleni S.M.J., Khalesi M.R. et al. Ammonia Leaching: A New Approach of Copper Industry in Hydrometallurgical Processes // J. Inst. Eng. India Ser. D. 2014. V. 94. P.95. https://doi.org/10.1007/s40033-013-0029-x.

Velásquez-Yévenes L., Ram R. The aqueous chemistry of the copper-ammonia system and its implications for the sustainable recovery of copper // Cleaner Engineering and Technology. 2022. V. 9. 100515. https://doi.org/10.1016/j.clet.2022.100515.

Wang Xi, Chen Qiyuan, Huiping Hu et al. Solubility prediction of malachite in aqueous ammoniacal ammonium chloride solutions at 25 °C // Hydrometallurgy. 2009. V. 99. P. 231–237. https://doi.org/10.1016/j.hydromet.2009.08.011.

Verchenko P.A., Setkova T.V., Spivak A.V., Zakharchenko E.S. Raman spectroscopy of synthetic co-bearing tourmaline. *UDC 549.612;543.424.2*

Korzhinskii Institute of Experimental Mineralogy RAS, Chernogolovka yapoletta@mail.ru

Abstract. Synthesis and analysis of new analogues of minerals belonging to the supergroup of tourmaline are aimed at studying their crystallochemical characteristics and development of materials with specified physical and chemical properties. In this work, Co-bearing tourmaline was synthesized in the hydrothermal settings at a temperature gradient of 400/550°C and pressure 100 MPa with boron-chloride hydrothermal solutions. As a result of the experiments, the dark pink overgrown layer up to 800 μm in size was obtained on the seed of natural elbaite crystal. The overgrown layer is characterized by zonal distribution of elements, with cobalt content varying from 12.37 to 16.86 wt.% CoO. The Raman-spectra in the range of 100-1500 cm^{-1} were obtained for the synthesized compound, and a comparative analysis with the spectrum of natural elbaite was performed. The influence of Co incorporation into the structure of tourmaline on its spectroscopic characteristics was determined. with wave number values ~ 268 cm^{-1} and ~ 446 cm^{-1} in the range *Y*-O and *Z*-O octahedral bonds, which are not representative of natural elbaite seed, were detected.

***Keywords**: tourmaline; Raman-spectroscopy; hydrothermal synthesis; cobalt; crystal structure*

Introduction. Tourmalines are widespread borosilicate minerals with complex crystal structures and variable chemical compositions. The general structural formula of the tourmaline supergroup minerals can be represented as $XY_3Z_6(T_6O_{18})(BO_3)_3V_3W$, where $X = Na^+$, Ca^{2+}, K^+ □ (= vacancy); *Y* – octahedral position occupied by Fe^{2+}, Mg^{2+}, Mn^{2+}, Al^{3+}, Li^+, Fe^{3+}, and Cr^{3+} atoms; *Z* – distorted octahedra occupied by Al^{3+}, Fe^{3+}, Mg^{2+}, and Cr^{3+} cations; *T* – tetrahedral position, can be occupied by Si^{4+}, Al^{3+}, and B^{3+} atoms; $V = OH^{1-}$ and O^{2-} and $W = OH^{1-}$, F^{1-}, and O^{2-}(Henry et al. 2011). The greatest compositional variation is observed at the *X, Y, Z, W,* and *V* sites. At the same time, tourmalines are considered as solid solutions with many isomorphic substitutions, which lead to

numerous end-members and make the crystallochemistry difficult to be fully described (Bosi et al. 2005). In this regard, the actual task of experimental mineralogy is to obtain new laboratory analogues of tourmaline in order to study their structural characteristics and possibilities of synthesis of this class of compounds to develop new materials with specified properties. Currently, synthetic analogues of tourmaline with dominant cations of Pb, Ag, La, Co, Ga, Ge, Sn, etc. have been obtained (Voskresenskaya et al. 1973; London 2011; Setkova et al. 2019, 2021; Vereshchagin et al. 2020, 2021). They can form separate mineral species but are not yet found in nature in sufficient quantities. Among them, synthetic Co-bearing tourmaline is of considerable interest due to its colouration, simplified composition and structural characteristics.

Raman spectroscopy is a powerful tool to investigate long-range and short-range bonds in crystal structures, this method provides additional information about the bonds between different crystallographic positions. In the presented work, the spectroscopic characteristics of Co-bearing tourmaline are studied.

Materials and methods. Synthesis of the studied Co-bearing tourmalines was carried out in the temperature range 400-550°C and pressures 100-150 MPa under thermogradient conditions with the contribution of boron-chloride hydrothermal solutions (Setkova et al., 2009). Boric acid (H_3BO_3) with concentration from 5 to 20 wt. %, sodium chloride (NaCl) with concentration from 5 to 15 wt. % and cobalt chloride crystallohydrate ($CoCl_2$-$6H_2O$) with concentration up to 30 wt. % were used for preparation of boron-chloride solutions. A natural elbaite seed of the Malkhansky deposit (Transbaikalia) was used.

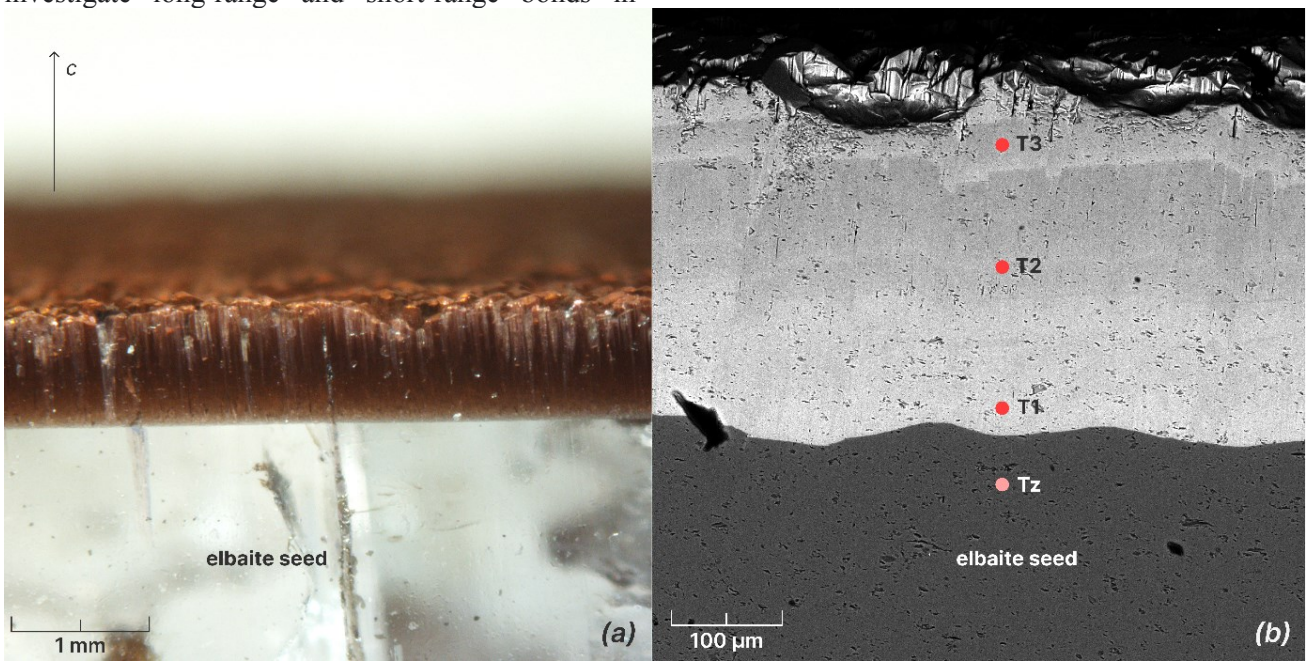

Fig. 1. (a) – an overgrown Co-tourmaline layer formed on the surface of natural elbaite seed; (b) – SEM-image of zonal crystal of Co-tourmaline layer

Table 1. Chemical composition of the seed crystal (Tz) and the overgrown layer of Co-bearing tourmaline (T1-T3).

Component	Composition in wt%				*Apfu* on 15 cations *Y*+*Z*+*T*=15 Kt			
	Tz	T1	T2	T3		T1	T2	T3
SiO_2	37.29	28.31	32.58	33.86	Si	5.18	5.71	5.79
Al_2O_3	37.92	32.74	35.23	37.27	Al	7.06	7.28	7.51
CoO	-	16.86	14.24	12.37	Co	2.77	2.00	1.70
Na_2O	1.11	1.49	0.97	0.85	Na	0.53	0.33	0.28
CaO	1.97	-	-	-	Ca	-	-	-
$B_2O_{3\ cal.}$	-	9.51	9.92	10.17	B	3	3	3
$H_2O_{\ cal.}$	-	2.74	2.60	2.96	OH	3.98	3.96	3.62
Σ	78.29	**91.65**	**95.54**	**97.48**	O	0.02	0.04	0.38

The chemical composition of the samples was determined on polished carbon-sprayed surfaces using a Tescan Vega II XMU scanning microscope with an INCA Energy 450 energy dispersive spectrometer (EDS). Raman spectra were obtained on a Renishaw instrument (RM1000) equipped with a Leica microscope using a λ = 532nm solid state laser, spectra were recorded at 50x magnification for 100s, in the range 100-1500 cm^{-1}.

Results and discussion. A sample of a dark pink Co-bearing tourmaline was selected for spectroscopic study (Fig. 1a). The overgrown layer reaches 800 μm thick and is characterised by zonal distribution of elements (Fig. 1b). The cobalt content in the newly formed layer decreases moving away from the elbaite seed boundary to the periphery, while the aluminum and silicon contents increase in this direction. Three zones (points T1, T2, T3) and the seed Tz can be distinguished by chemical composition (Table 1).

According to previously published structural data for Co-bearing tourmaline (Rozhdestvenskaya et al. 2012) of composition close to point (T2), the refined crystallochemical formula is: $Na_{0.35}(Al_{1.80}Co_{1.20})(Al_{5.28}Co_{0.66}Ti_{0.06})(Si_{5.64}B_{0.36})O_{18}(BO_3)_3(OH)_{3.81}O_{0.19}$, with cobalt cations occupying both *Y*– and *Z*–sites, and a small amount of boron was found to be incorporated into the tetrahedral *T*-site.

Factor group analysis of tourmalines predicts 28 *Ag* and 49 *Eg* Raman-active modes. In this study, on unpolarised spectra in the range 100 – 1500 cm^{-1}, 14 vibrations for elbaite and 16 vibrations for Co-tourmaline with different intensities were detected. The Raman spectra measured from the points of three compositions (T1, T2, T3) of Co-bearing tourmaline and elbaite seed (Tz) are presented in Fig. 2.The wavenumbers of the observed bands (cm^{-1}) and their attribution to the corresponding types of vibrations according to previously published works (Gasharova et al, 1997; Watenphul et al, 2016; Spivak et al, 2021) are given in Table 2.

In the range of 150-1500 cm^{-1} there are distinguished regions with corresponding vibrations: <160 cm^{-1} – vibrations of atoms in the *X*-site (Spivak et al, 2021), 160-280 cm^{-1} – vibrations associated with YO_6 octahedra (Gasharova et al, 1997; Watenphul et al), 280-460 cm^{-1} – vibrations associated with ZO_6 octahedra (Gasharova et al, 1997; Watenphul et al), 460-670 cm^{-1} – oxygen vibrations in Si_6O_{18} rings (Spivak et al, 2021), 670-750 cm^{-1} – vibrations associated with BO_3 groupings (Gasharova et al, 1997), 750-840 cm^{-1} – vibrations of B-O-Al bonds (Gasharova et al, 1997), 840-1100 cm^{-1} – internal vibrations of SiO_4 tetrahedra (Watenphul et al, 2016) (Fig. 2).

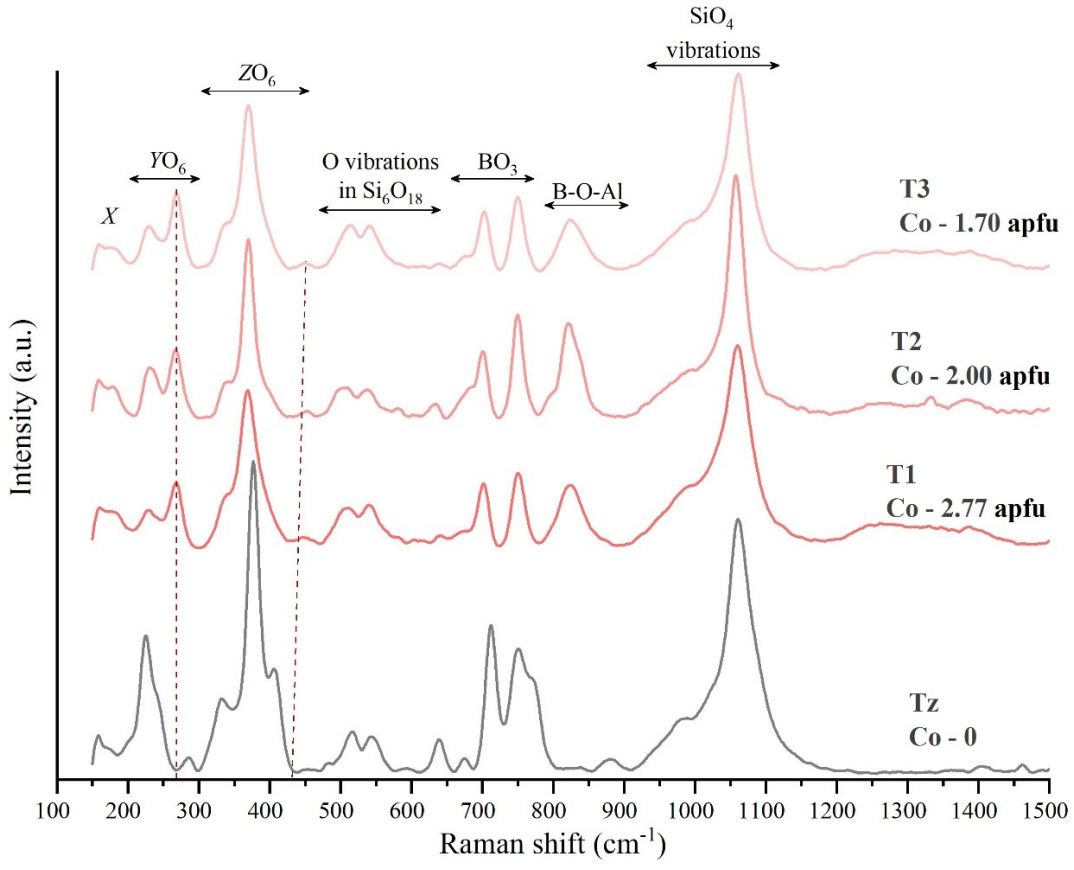

Fig. 2. Unpolarized Raman spectra of synthesized crystals at three points – filmed as they are distant from the elbaite seed

In comparison with natural elbaite seed, an additional band at ~ 267-269 cm^{-1} is observed in the region of YO_6 octahedra vibrations for Co-bearing tourmaline. Its position shifts by ~2 cm^{-1} towards higher values of wavenumbers with increasing cobalt content in the tourmaline composition (Table 2). Correspondingly, this band can be attributed to vibrations of Co-O bonds in octahedrons. An additional band at ~450 cm^{-1} of low intensity is also observed in the region of ZO_6 octahedral vibrations (Table 2), which may indicate that cobalt also enters the *Z*-site. The range of wavelength values from ~670 to ~840 cm^{-1} belongs to internal vibrations of BO_3 groups and vibrations of B-O, O-B-O and B-O-Al bonds. In this region in Co-containing tourmaline an additional band at ~ 825 cm^{-1} is observed, the appearance of which may be associated with the entry of boron and/or aluminium atoms into the tetrahedral position and indicate vibrations of the B-O-Al type. In our case, the presence of boron and/or aluminium in Co-bearing tourmaline in the *T*-site is confirmed by the reduced silicon content in the composition (Table 1). An intense peak in the region from 950 to 1060 cm^{-1} is present both in the elbaite seed and in the accreted word and corresponds to the vibrations of Si-O bonds in SiO_4 tetrahedra.

Table 2. Wave numbers of the observed bands (cm^{-1}) in the Raman spectroscopy for seed crystal (Tz) and Co- bearing tourmaline (T1-T3)

Tz	T1	T2	T3	Points of the measured spectra
0	2.77	2.00	1.70	Co content (apfu)
156	158	155	158	*X*-cation translations
168	176	180	176	YO_6 bending vibrations
225	228	232	235	
	269	**268**	**267**	***Y*-O (Co-O) bending vibrations**
285				O-Al-O bending vibrations
334	333	335	336	Si-Onon rck
377	370	374	370	ZO_6 bending vibrations
	448	**446**	**451**	***Z*-O (Co-O) bending vibrations**
513	510	507	504	Oxygen vibrations in Si – O rings
544	544	542	538	
639	639	640	632	Si-O_{br} rck
674	678	676	685	B-O str & B-O-Al bend
712	703	702	702	BO_3 bending vibrations
750	750	751	750	B-O stretching vibrations B-O-Al bend
	827	**825**	**825**	B-O-Al bending vibrations
979	1024	1045	1031	Si- O_{non} stretching vibrations
1059	**1061**	**1061**	**1058**	Si – O_{br} asym.stretching Si-O-Si, Si – O_{non} asym. stretching

O_{br}, bridging oxygens in the Si-O rings, which link two SiO_4 tetrahedra;
O_{non}, non-bridging oxygens in the Si-O rings.

Conclusion. Thus, a synthetic analogue of cobalt-bearing tourmaline (up to 16.86% CoO or 2.77 apfu of Co) was obtained by hydrothermal method at T = 500/550°C and P = 100MPa in the form of an overgrowth layer on elbaite seed. The Raman spectra of the natural elbaite seed and the grown layer of Co-rich tourmaline were obtained in the range of 150-1500 cm^{-1} with bands of different intensities. The most intense bands were assigned to the corresponding types of framework vibrations.

Additional bands at ~ 268 cm^{-1} and ~ 450 cm^{-1}, which can be related to vibrations of Co–O bonds in octahedra, were found in the spectra of Co-containing tourmaline.

The spectroscopic characteristics confirm earlier structural data (Rozhdestvenskaya et al., 2012), according to which cobalt cations populate not only the *Y*-site but also the *Z*-site, and boron ions partially populate the tetrahedral position in addition to the triangular coordination.

Acknowledgements

The research was supported by RNF grant No. 25-27-00194 https://rscf.ru/project/25-27-00194/

References

Bosi F. Andreozzi G. B., Federico M., Graziani G., Lucchesi S. Crystal chemistry of the elbaite-schorl series // American Mineralogist. 2005. V. 90. №. 11-12. P. 1784-1792. https://doi.org/10.2138/am.2005.1827

Gasharova B., Mihailova B., Konstantinov L. Raman spectra of various types of tourmaline // European Journal of Mineralogy. 1997. V. 9. №. 5. P. 935-940. https://doi.org/10.1127/ejm/9/5/0935.

Henry, D. J., Novak, M., Hawthorne, F. C., Ertl, A., Dutrow, B. L., Uher, P., & Pezzotta, F. Nomenclature of the tourmaline-supergroup minerals // American Mineralogist. 2011. V. 96. №. 5-6. P. 895-913. https://doi.org/10.2138/am.2011.3636

London D. Experimental synthesis and stability of tourmaline: a historical overview // The Canadian Mineralogist. 2011. V. 49. №. 1. p. 117-136. https://doi.org/10.3749/canmin.49.1.117

Rozhdestvenskaya I.V., Setkova T.V., Vereshchagin O.S., Shtukenberg A.G., Shapovalov Yu.B. Refinement of Crystal Structures of Synthetic Nickel- and Cobalt-Containing Tourmalines // Kristallografiya. 2012. Vol. 57, No. 1, p. 63.

Setkova T., Balitsky V., Shapovalov Y. Experimental study of the stability and synthesis of the tourmaline supergroup minerals // Geochemistry International. 2019. V. 57. №. 10. P. 1082-1094. https://doi.org/10.31857/s0016-752564101064-1078

Setkova T., Borovikova, E., Spivak, A., Balitsky, V. Crystal growth and Raman spectroscopy of Ga, Ge-rich tourmaline. // Grafica editoriale. 2021. P. 97.

Setkova T.V., Shapovalov Yu.B., Balitsky V.S. // Doklady RAN. 2009. Vol. 424, No. 1, p. 94.

Spivak A., Borovikova E., Setkova T. Raman spectroscopy and high pressure study of synthetic Ga, Ge-rich tourmaline // Spectrochimica Acta Part A: Molecular and Biomolecular Spectroscopy. 2021. V. 248. P. 119171. https://doi.org/10.1016/j.saa.2020.119171

Vereshchagin O., Wunder B., Britvin S., Frank-Kamenetskaya O., Wilke F.D.H., Vlasenko N., Shilovskikh V. Synthesis and crystal structure of Pb-dominant tourmaline // American Mineralogist. 2020. V. 105. №. 10. P. 1589-1592. https://doi.org/10.2138/am-2020-7457

Vereshchagin O., Britvin S, Wunder B., Frank-Kamenetskaya O., Wilke F.D.H., Vlasenko N., Shilovskikh V., Bocharov V., Danilov D. Ln^{3+} (Ln^{3+} = La, Nd, Eu, Yb) incorporation in synthetic tourmaline analogues: Towards tourmaline REE pattern explanation // Chemical Geology. 2021. V. 584. P. 120526 https://doi.org/10.1016/j.chemgeo.2021.120526

Voskresenskaya I.E., Sternberg L.A. Synthesis of Tourmaline in Chloride Media // Kristallografiya. 1973. Vol. 19, No. 4, pp. 888-890.

Watenphul A., Schlüter J., Bosi F., Skogby H., Malcherek T., Mihailova B. Influence of the octahedral cationic-site occupancies on the framework vibrations of Li-free tourmalines, with implications for estimating temperature and oxygen fugacity in host rocks // American Mineralogist. 2016. V. 101. №. 11. P. 2554-2563. https://doi.org/10.2138/am-2016-5820.